Covalent ERα Antagonist H3B-6545 Demonstrates Encouraging Preclinical Activity in Therapy-Resistant Breast Cancer

Craig Furman[1], Xiaoling Puyang[1], Zhaojie Zhang[1], Zhenhua J. Wu[1], Deepti Banka[1], Kiran B. Aithal[2], Lee A. Albacker[3], Ming-Hong Hao[1], Sean Irwin[1], Amy Kim[1], Meagan Montesion[3], Alyssa D. Moriarty[4], Karthikeyan Murugesan[3], Tuong-Vi Nguyen[1], Victoria Rimkunas[1], Tarek Sahmoud[1], Michael J. Wick[4], Shihua Yao[1], Xun Zhang[1], Hao Zeng[1], Frédéric H. Vaillancourt[1], David M. Bolduc[1], Nicholas Larsen[1], Guo Zhu Zheng[1], Sudeep Prajapati[1], Ping Zhu[1], and Manav Korpal[1]

ABSTRACT

Nearly 30% of patients with relapsed breast cancer present activating mutations in estrogen receptor alpha (ERα) that confer partial resistance to existing endocrine-based therapies. We previously reported the development of H3B-5942, a covalent ERα antagonist that engages cysteine-530 (C530) to achieve potency against both wild-type ($ERα^{WT}$) and mutant ERα ($ERα^{MUT}$). Anticipating that the emergence of C530 mutations could promote resistance to H3B-5942, we applied structure-based drug design to improve the potency of the core scaffold to further enhance the antagonistic activity in addition to covalent engagement. This effort led to the development of the clinical candidate H3B-6545, a covalent antagonist that is potent against both $ERα^{WT/MUT}$, and maintains potency even in the context of ERα C530 mutations. H3B-6545 demonstrates significant activity and superiority over standard-of-care fulvestrant across a panel of $ERα^{WT}$ and $ERα^{MUT}$ palbociclib sensitive and resistant models. In summary, the compelling preclinical activity of H3B-6545 supports its further development for the potential treatment of endocrine therapy–resistant $ERα^{+}$ breast cancer harboring wild-type or mutant *ESR1*, as demonstrated by the ongoing clinical trials (NCT03250676, NCT04568902, NCT04288089).

Summary: H3B-6545 is an ERα covalent antagonist that exhibits encouraging preclinical activity against CDK4/6i naïve and resistant $ERα^{WT}$ and $ERα^{MUT}$ tumors.

Introduction

A large fraction of breast cancers are dependent on estrogen receptor alpha (ERα) signaling for their oncogenic growth. The development of therapies that reduce ERα pathway activity, either by blocking synthesis of estrogens or through direct targeting of estrogen receptor, has proven to be a highly effective strategy for treating a subset of $ERα^{+}$ breast cancer. Unfortunately, innate and acquired resistance to these ER-directed therapies hinders efficacy, leading to poor clinical outcomes. One mechanism of escape found in nearly 30% of resistant metastases is mutations of ERα, resulting in ligand-independent activation of the ERα pathway (1–3). Because a significant proportion of endocrine-resistant metastases remain dependent on ERα signaling and existing endocrine therapies exhibit reduced efficacy against ERα mutations, there is a pressing need to develop next-generation ERα antagonists that can effectively suppress residual $ERα^{MUT}$ activity. Recent efforts have focused on developing selective estrogen receptor degraders (SERDs) that are orally bioavailable with better pharmacokinetic properties than fulvestrant. Indeed, several oral SERDs, including RAD1901 (Elacestrant), GDC-9545 (Giredestrant), SAR439859 (Amcenestrant), and AZD9833 (Camizestrant), have exhibited both preclinical and clinical antitumor activity in the $ERα^{WT}$ and $ERα^{MUT}$ settings (4–12). Despite these promising results, there remains an opportunity to develop ERα antagonists with novel modes of action, potentially capable of more effective suppression of $ERα^{MUT}$ activity.

Recently we described the development of H3B-5942, a member of a novel class of ERα antagonist that potently inhibits $ERα^{WT}$ and several common ERα mutations by covalently targeting a unique cysteine residue [cysteine-530 (C530)] (13). However, because the potency of H3B-5942 is critically dependent on covalency (13), it is possible that C530 mutations could serve as an escape mechanism in the therapeutic setting. With this potential liability in mind, we developed H3B-6545, an antagonist with improved potency of the core scaffold to further enhance the antagonistic activity in addition to covalent engagement (14). H3B-6545 exhibits favorable drug-like properties and demonstrates significant preclinical activity, with single-digit nanomolar potency *in vitro* and superiority over fulvestrant *in vivo* across CDK4/6i naïve and resistant $ERα^{WT}$ and $ERα^{MUT}$ models. These promising preclinical data support further development of this novel class of antagonist for treatment of patients with $ERα^{+}$, $HER2^{-}$ breast cancer (NCT03250676, NCT04568902, NCT04288089).

[1]H3 Biomedicine Inc., Cambridge, Massachusetts. [2]Aurigene Discovery Technologies Ltd, Bangalore, Karnataka, India. [3]Foundation Medicine Inc., Cambridge, Massachuetts. [4]START, Preclinical Research, San Antonio, Texas.

Note: Supplementary data for this article are available at Molecular Cancer Therapeutics Online (http://mct.aacrjournals.org/).

C. Furman, X. Puyang, and Z. Zhang contributed equally to this article.

Corresponding Authors: Craig Furman, H3 Biomedicine, 300 Technology Square, Cambridge, MA 02139. E-mail: craig_furman@h3biomedicine.com; Manav Korpal, manav_korpal@h3biomedicine.com; and Ping Zhu, ping_zhu@h3biomedicine.com

Mol Cancer Ther 2022;21:890–902

doi: 10.1158/1535-7163.MCT-21-0378

Materials and Methods

Synthetic procedures

Synthesis of H3B-5942 and H3B-9224 has been described in Discovery of Selective Estrogen Receptor Covalent Antagonists for the treatment of ERα^{WT} and ERα^{MUT} breast cancer. Puyang and colleagues Cancer Discov July 10 2018 **DOI:** 10.1158/2159-8290.CD-17-1229 (13).

Synthesis of H3B-6545 has been described in Bock, M. and colleagues (2017) United States Patent No. US 9,796,683 B2, Example 60 (14).

Synthesis of H3B-9709 has been described i*n* Bock, M. (2018) United States Patent Application Publication No. US 2018/0141913 A1, Example 2 (15).

Cell lines

MCF7 BUS cells (16) and MCF7-derived lines engineered to overexpress mutant forms of ERα were maintained in DMEM supplemented with 10% FBS, 4 mmol/L L-glutamine and 1× non-essential amino acids. The patient-derived xenograft (PDX)-ER$\alpha^{Y537S/WT}$ ST941 cell line was derived from a PDX tumor model and was routinely cultured in DMEM supplemented with 20% FBS. Lenti-X 293T cells (Clontech, catalog no. 632180) were cultured in DMEM supplemented with 10% FBS and 4 mmol/L L-glutamine. All cells were maintained prior to and during experiments at 37°C, 5% CO_2, and at 95% relative humidity. Cells were passaged two to three times per week and discarded when the passage number exceeded 20. For *in vitro* experiments, cells were seeded at appropriate densities to provide logarithmic growth during, and at least 24 hours beyond, the experiment duration. The identities of all cell lines were confirmed by short tandem repeat analysis of nine markers and were verified to be free of Mycobacterium contamination before performing experiments.

Protein production, purification, and intact mass spectrometry

The various ERα protein constructs were expressed and purified as described previously (13). The covalent engagement by H3B-6545 was monitored by mass spectrometry after a 4°C overnight incubation essentially as described previously (13). For the time course experiment, the levels of covalently modified ERα were monitored at various incubation times at room temperature (0, 2.5, 5, 10, 15, 30, 45, 90 minutes). The reaction was quenched by diluting the sample in 0.1% formic acid in water and analyzed as described previously (13). The fits and k_{obs} values were determined using the GraphPad Prism software.

Crystallography

His-TEV-ERα^{Y537S} (307-554) was cloned into pET-28a (EMD Millipore) and expressed in *E. coli*. In this construct, two surface exposed cysteine mutations, C381S and C417S, were introduced to improve protein behavior and yields. Soluble protein was obtained by overnight induction at 20°C using 0.1 mmol/L IPTG (17). Cells were harvested and protein was purified using Ni-NTA chromatography followed by overnight TEV cleavage of the His-tag and a polishing subtractive Ni-NTA step to remove the TEV. The flow-through was concentrated and injected on a sephacryl S-300 column equilibrated in 50 mmol/L Tris pH 8, 150 mmol/L NaCl, 1 mmol/L TCEP, and 10% glycerol. Peak fractions were pooled and concentrated to approximately 12.4 mg/mL and flash frozen in liquid nitrogen. Cocrystals were obtained by mixing compound and protein at 2:1 molar ratio at room temperature for 1 hour to allow time for covalent bond formation, followed by filtration to remove aggregates. Sitting drops were set up using 0.5 μL protein + 0.5 μL reservoir and equilibrated over a reservoir containing 40% PEG 1000, 60 mmol/L NaCl, and 100 mmol/L TAPS pH 9. Crystals grew to full size in 1–3 weeks and flash frozen using reservoir solution supplemented with 10% ethylene glycol. Data were collected by HarkerBIO at the Diamond Light Source, beamline I04. The structure was solved by molecular replacement using MOLREP (18) and refined using Refmac (19) with ligand coordinates generated using Schrodinger. The PDB identification code for H3B-6545 is 6OWC.

Jump dilution experiments

The jump dilution experiments using unlabeled compound and ^{3}H-E2 were performed as described previously (13). The jump dilution experiment using ^{3}H-H3B-9709 was performed by incubating 30 nmol/L ERα protein with 75 nmol/L ^{3}H-H3B-9709. After a 5-hour incubation, the mixture was diluted 20-fold and 200 nmol/L of unlabeled E2 was added to half the samples. The diluted sample was further incubated for 22 hours at 4°C followed by binding to the HAP resin and scintillation counting as described previously (13).

Intact mass spectrometry to assess covalency of H3B-6545

ERα wild-type (297-554) and mutant proteins (297-554) were incubated in 50 mmol/L Tris pH 8.0, 150 mmol/L NaCl, 5% glycerol, and 1 mmol/L TCEP with a 2-fold excess of compound (2 μmol/L H3B-6545: 1 μmol/L ERα protein solution) at 4°C overnight. Mass analyses were carried out on a Thermo Fisher Scientific Q-Exactive HRM (ESI source, 4.0 kV ionization voltage, 250°C capillary temperature, 10 arb sheath gas, S-lens RF level 65) coupled with an Accela Open AS 1250. Samples (10 μL) were desalted on a C4 column (Thermo Fisher Scientific Accucore 2.1 × 150 mm, 2.6 μm) with a gradient from 5% to 95% B over 10 minutes. Eluent A consisted of 0.1% formic acid in water, and eluent B consisted of 0.1% formic acid in acetonitrile. The flow was set to 400 nL/minute. All solvents were LC/MS grade (Thermo Fisher Scientific). The mass spectrometer was run in positive mode collecting full scan at $R = 70{,}000$ from m/z 500 to m/z 2,000. Data were collected with the Xcalibur 3.1 software. Xcalibur raw files were processed using BioPharma Finder 2.0 (Thermo Fisher Scientific) and the ReSpect deconvolution algorithm. The peak was averaged over the selected retention time to generate source spectra from the TIC chromatogram trace, and the chromatogram parameters set to m/z 700 to 2,000. Outputs from the deconvolution algorithm include model mass range from 10,000 to 160,000, mass tolerance 20 ppm, charge state range from 10 to 100. The target mass is the estimated mass of protein or protein + compounds, with noise rejection of 95% confidence.

Monitoring of covalent protein labeling using tritiated compounds

The incorporation of a ^{3}H-dimethylamino group in H3B-6545 and H3B-9709 was performed at Moravek Biochemicals Inc. Specific activities of 26.0 and 15.1 Ci/mmol/L were obtained, respectively. The monitoring of covalent protein labeling was performed by incubating 750 nmol/L ^{3}H-H3B-6545 or 150 nmol/L ^{3}H-H3B-9709 with 60 nmol/L ERα at room temperature in a 750 μL reaction volume. At various timepoints (0, 5, 15, 30, 60, and 120 minutes) 75 μL of the reaction was removed and quenched with 30 μL 4 N HCl for 10 minutes. ERα protein was then precipitated with 700 μL tricarboxylic acid (TCA; 10% final). The samples were centrifuged and washed once with 500 μL 10% TCA, and the protein pellet containing covalently bound radiolabeled compound was resolubilized in 500 μL 88% formic acid and quantified by liquid scintillation counting. The fits and k_{obs} values were determined using the GraphPad Prism software.

Immunoblot analysis in whole-cell lysates

Cells were lysed in loading buffer (Invitrogen, catalog no. NP0007) containing protease inhibitor (Roche, catalog no. 05892791001) and DTT (Invitrogen, catalog no. NP0009), sonicated and subsequently boiled for 5 minutes. Approximately 30 μg of protein was loaded per lane and resolved by SDS polyacrylamide electrophoresis. Protein was transferred onto nitrocellulose membranes, blocked in 5% low-fat milk and probed overnight with antibodies to ER (SP1; Spring Bioscience, catalog no. M3012), α−Tubulin (Sigma, catalog no. T6199) or GAPDH (Sigma, catalog no. G9545). Membranes were incubated with horseradish peroxidase–conjugated anti-rabbit secondary antibody (Cell Signaling Technology, catalog no. 7074) or anti-mouse secondary antibody (Cell Signaling Technology, catalog no. 7076) for 1 hour and signal was developed using the ECL method (GE Healthcare).

RNA extraction and quantitative real-time PCR analysis

Total RNA was extracted using the RNeasy Mini Kit (QIAGEN, catalog no. 74104) according to the manufacturer's instructions and cDNA was made using the High Capacity cDNA Reverse Transcription Kit (Applied Biosystems, catalog no. 4374966. Following completion of the RT reaction, qPCR reactions were set up in triplicate for each biological replicate using the TaqMan Gene Expression Master Mix (Applied Biosystems, catalog no. 4370074) and gene-specific probes *GREB1* (Hs00536409_m1/FAM) or PGR (Hs201556702_m1/FAM. *GAPDH* (Hs02758991_g1/VIC_PL) or GUSB (Hs.PT.58v.27737538/Cy5) served as the endogenous control.

RNA-sequencing analysis

MCF7 parental cells were treated with various compounds at 100 nmol/L. Media and compounds were refreshed after 3 days, and cell lysates were collected 6 days following treatment initiation in TRIzol and immediately frozen with liquid nitrogen prior to analysis. Cell cultures were in log phase growth for the duration of the experiment.

For principal component analysis, TPM values were subjected to logarithmic transformation calculated by Kallisto v0.43.0 (20). Genes with maximum TPM values < 1 across all samples and genes with mean absolute deviation (MAD) values < 0.2 were filtered out.

For differential gene expression analysis of RNA-sequencing data, the read count values estimated by Kallisto (20) were used as input for the differential expression analysis. TMM in R package edgeR (21) was used for normalization, and limma voom (22) was used for differential gene analysis. Fold change of 2 and adjusted *P* value of 0.05 was used as the cutoff to call significantly differential expressed genes, which were used for the Venn diagram presented in Supplementary Fig. S4B.

Single-dose pharmacokinetic and pharmacodynamics tumor analysis and efficacy study in MCF7 xenograft model

The ERα wild-type human breast cancer cell line MCF7(P)-AP2, a serially *in vivo* passaged cell line derived from the MCF7-ATCC tumors at Aurigene Discovery Technologies Limited, was cultured in EMEM supplemented with 10% FBS at 37°C in a 5% CO_2 atmosphere and kept in the exponential growth phase as described previously (13). For harvesting, the cells were washed with PBS, incubated with 0.25% trypsin-EDTA, and suspended in a 1:1 mixture of Matrigel (Corning 354234) and Hank's Balanced Salt Solution at a final concentration of 5×10^7 cells/mL. To generate xenografts, 0.2 mL of the inoculum was injected into the third mammary fat pad of 6–8 weeks old female Balb/c nude mice (6–8 weeks old, Balb/cOlaHsd-*Foxn1*^{nu}), giving a final concentration of 1×10^7 cells/mouse. Three days prior to inoculation, mice were implanted with 0.72 mg, 90-day release estrogen pellets (Innovative Research of America). For pharmacokinetic and pharmacodynamic analysis, tumors were allowed to reach an average volume of approximately 300 mm^3 prior to randomization ($N = 3$/group). H3B-6545 at 1, 3, 10, or 30 mg/kg was administered once (QD×1) by oral gavage. Tumor xenografts were collected at 1, 2, 4, 8, 24, 48, and 72 hours postdose. The oral administration volume [10 mL/kg body weight (BW)] was calculated from the BW prior to compound administration. All procedures relating to animal care, handling, and treatment were performed in accordance and with the approval of the Institutional Animal Ethics Committee of Aurigene Discovery Technologies Ltd. All doses were well tolerated with no clinical signs observed in all studies presented. For plasma bioanalysis, samples from vehicle groups (0 mg/kg) and H3B-6545-treatment groups were placed in K_2EDTA tubes on wet ice until centrifugation (within 30 minutes of sample collection). Following centrifugation, two aliquots of plasma were transferred into uniquely labeled polypropylene tubes, prior to being flash frozen. Tumor samples for bioanalysis and PCR studies were immediately snap-frozen and stored at −80°C. Plasma and tumor samples were analyzed at Aurigene Discovery Technologies Limited.

For the efficacy study, treatments were initiated once the average tumor volume reached approximately 200 mm^3 and the study was terminated on day 17. BW was measured daily whereas tumor volume (TV) was measured twice a week.

Repeat dose pharmacokinetic and pharmacodynamic tumor analysis and efficacy study in the ST941 PDX model

The ST941 PDX model representing an ER$\alpha^{Y537S/WT}$-mutated human ER-positive (ER^+) breast cancer was propagated in athymic Nude mice. To generate patient-derived xenografts, solid tumor tissues from the ER$\alpha^{Y537S/WT}$-positive xenograft model were cut into 70 mg pieces, mixed with Matrigel (Corning, 354234) and subcutaneously implanted into the right flank of 12-week-old female athymic Nude (Crl:NU(NCr)-Foxn1nu) mice supplied with drinking water containing E2 (Sigma-Aldrich, catalog no. E1024-25G). When the mean TV reached approximately 300 mm^3, animals were selected on the basis of TV and randomized into treatment groups of 3 animals per group for the pharmacokinetic and pharmacodynamic analysis. Beginning three days prior to treatment and for the remainder of the studies, exogenous E2 was removed from the drinking water. H3B-6545 was administered orally QD×5 at 3, 10, 30, and 100 mg/kg. Plasma and tumor xenografts were collected at 1, 2, 4, 8, 24, 48, and 72 hours postdose. The oral administration volume (10 mL/kg BW) was calculated from the BW prior to compound administration. Plasma and tumor pharmacokinetic analyses were performed at Agilux Laboratories Inc.

For the efficacy studies, when the mean TV reached approximately 200 mm^3, animals were selected on the basis of TV and randomized into treatment groups. Tamoxifen was given subcutaneously TIW, H3B-6545, and palbociclib were dosed orally once daily, whereas fulvestrant was given subcutaneously once weekly. Each treatment was administered on the basis of BW (10 mL/kg), except tamoxifen and fulvestrant, which were flat dosed (both formulated as described above). Beginning 3 days prior to treatment and for the remainder of the studies, exogenous E2 was removed from the drinking water. BW measurements were performed daily and TV measurements were recorded twice per week. All studies were performed under guidelines and with the approval of the START Institutional Animal Care and

Use Committee (IACUC) and defined in the START Animal Care and Use Program (Protocol 09-001). All doses and regimens were well tolerated.

End-of-study tumor samples were formalin-fixed and paraffin-embedded (FFPE) at START and subsequently shipped to Cancer Genetics Inc. for sectioning, and staining. In brief, 5-μm sections of FFPE tissue xenograft samples were stained for PR and Ki67 using the Ventana rabbit monoclonal primary antibodies ER (SP1), progesterone receptor (PR; 1E2), and Ki-67 (30-9). IHC assays were run on the Ventana BenchMark IHC/ISH automated slide staining instrument with *ultra*View Universal DAB detection kit. PR and Ki-67 stained slides were scored for % positive tumor cells by a board certified MD pathologist at Cancer Genetics Inc. Scanned images, pathologist scores, and interpretations were made available to H3 Biomedicine Inc., for review and data analysis.

ERα^{WT} ST986 and ST1799 PDX tumor xenograft generation, dosing, and measurement of antitumor activity

The ST986 and ST1799 PDX models representing ERα^{WT} human ER$^+$ breast cancer were propagated in female athymic Nude mice. To generate PDXs, solid tumor tissues from the ERα^{WT} xenograft models were cut into 70 mg pieces, mixed with Matrigel (Corning, 354234), and subcutaneously implanted into the right flank of 12-week-old female athymic Nude (Crl:NU(NCr)-Foxn1nu) mice supplied with drinking water containing E2 (Sigma-Aldrich, catalog no. E1024-25G). When the mean TV reached approximately 125–200 mm^3, animals were selected on the basis of TV and randomized into treatment groups. H3B-6545 was administered orally once daily, tamoxifen was given subcutaneously three times a week, fulvestrant was given subcutaneously once weekly, and palbociclib was administered orally once daily. Each treatment was administered on the basis of BW (10 mL/kg), except tamoxifen and fulvestrant, which were flat-dosed. Tamoxifen was formulated in 90% peanut oil/10% ethanol, and clinical grade fulvestrant was administered without further dilution. Exogenous E2 was supplemented in the drinking water during the course of the study. BW measurements were performed daily and TV measurements were recorded twice per week. All studies were performed under guidelines and with the approval of the START IACUC and defined in the START Animal Care and Use Program (Protocol 09-001). All doses and regimens were well tolerated.

ERα^{Y537S} ST2177 PDX tumor xenograft generation, dosing, and measurement of antitumor activity

The ST2177 PDX model representing an ERα^{Y537S}-mutant human ER$^+$ breast cancer was propagated in mice. To generate PDXs, solid tumor tissues from the ERα^{Y537S} xenograft model were cut into 70 mg pieces, mixed with Matrigel (Corning, 354234), and subcutaneously implanted into the right flank of 7–12 weeks old female athymic Nude (Crl:NU(NCr)-Foxn1nu) mice supplied with drinking water containing E2 (Sigma-Aldrich, catalog no. E1024). When the mean TV reached approximately 125–200 mm^3, animals were selected on the basis of TV and randomized into treatment groups of 7–8 animals per group. H3B-6545 was administered orally once daily, and fulvestrant was given subcutaneously once weekly. Each treatment was administered on the basis of BW (10 mL/kg), except fulvestrant which were flat dosed. Exogenous E2 was supplemented in the drinking water during the course of the study. BW measurements were performed daily and TV measurements were recorded twice per week. All studies were performed under guidelines with the approval of the START IACUC and defined in the START Animal Care and Use Program (Protocol 09-001). All doses and regimens were well tolerated.

ERα^{Y537S} ST2056 PDX tumor xenograft generation, dosing, and measurement of antitumor activity

The ST2056 PDX model representing an ERα^{Y537S}-mutated human ER$^+$ breast cancer was propagated in mice. Efficacy study in ST2056 PDX model was performed as previously described for other PDX models (13). H3B-6545 was administered orally once daily, and clinical-grade fulvestrant was administered subcutaneously once weekly. BW measurements were performed daily, and TV measurements were recorded twice per week. Mice with at least 20% BW loss compared with day 0 BW were euthanized to prevent any pain or suffering to the animal. All studies were performed under guidelines and the approval of the START IACUC and defined in the START Animal Care and Use Program (Protocol 09-001). All doses and regimens were well tolerated.

ERα^{WT} ST1799-PBR and ERα$^{Y537S/WT}$ ST941-PBR PDX tumor xenograft generation, dosing, and measurement of antitumor activity

The ST1799-PBR and ST941-PBR palbociclib-resistant PDX models representing ERα^{WT} and ERα$^{Y537S/WT}$ human ER$^+$ breast cancer, respectively, were propagated in mice. To generate palbociclib-resistant models, palbociclib was continuously administered once the mean TV reached approximately 125–200 mm^3 until tumors reached approximately 2,000 mm^3. Fragments from the stable palbociclib-resistant tumors were implanted into study mice, H3B-6545 was administered orally once daily, fulvestrant was administered subcutaneously once weekly, and palbociclib was administered orally once daily. Exogenous E2 was supplemented in the drinking water during the course of the study for the ST1799-PBR model whereas E2 was removed 3 days prior to dosing in the ST941-PBR model. BW measurements were performed daily and TV measurements were recorded twice per week. All studies were performed under guidelines and with the approval of the START IACUC and defined in the START Animal Care and Use Program (Protocol 09-001). All doses and regimens were well tolerated.

Assessment of H3B-6545 effects on bone density and uterus in ovariectomized rats

Six-month-old female Sprague-Dawley rats (Charles River Canada) were randomly assigned to groups that underwent either sham or ovariectomy (OVX) surgery followed by a one month bone depletion period. At the end of the 1-month period, all ovariectomized rats received once daily oral gavage doses of vehicle control [0.5% (w/v) methylcellulose and 0.2% (w/v) Tween 80 in ultrapure water], H3B-6545 (3, 10, and 30 mg/kg/day in vehicle), 17β-estradiol (Sigma, 0.01 mg/kg/day in corn oil) or tamoxifen (Sigma, 1 mg/kg/day in corn oil) for 6 weeks ($N = 20$/group). Sham group ($N = 20$) received daily administration of vehicle solution as a negative control. Bone scans were performed on the right femur in all animals using dual energy X-ray absorptiometry (DXA). Scans were acquired once prior to initiation of dosing and once during the dosing period (week 5/6). Bone mineral density (BMD, g/cm^2) data derived from the scans were used to assess the effects of H3B-6545 on OVX-induced bone loss. At the end of the 6-week treatment period, all animals were euthanized. BW and uterus weight were recorded for each animal. Uterus tissues were collected and evaluated for histopathologic changes. For statistical analysis, pairwise comparisons were conducted between each treatment group and OVX control group using Dunnett test. Statistical significance is defined by $P < 0.05$. The conduct of the animal study followed the Standard Operating Procedure guidelines and approval by Charles River Montreal.

Statistical analysis

In vitro data are expressed as mean ± SEM or mean ± SD as indicated. Statistical significance was determined by two-sided *t* test analysis. Efficacy data are expressed as mean ± SEM for TV. The differences in TV on the final day of TV measurements between the vehicle and treatment groups were analyzed by multiple unpaired *t* tests with significance determined using the Holm-Sidak method with alpha set to 0.05 and without assuming a consistent SD. Statistical analyses were performed using GraphPad Prism version 5.04 (GraphPad Software).

Data availability

The data for the indicated studies are publicly available in Gene Expression Omnibus at GSE178373. The PDB identification code for H3B-6545 is 6OWC. All other data are available from the authors upon reasonable request.

Results

Development of H3B-6545

Previously we described H3B-5942, a first-in-class ERα antagonist that derives potency against both $ERα^{WT}$ and $ERα^{MUT}$ by forming a specific covalent bond with C530 of ERα (**Fig. 1A** and **B**; **Table 1**) (13). As previously shown, mutations in C530 do not significantly impact basal or estradiol (E2)-mediated ERα function (13, 23), but they may confer resistance to this class of covalent inhibitors. With this potential liability in mind, we aimed to develop an improved antagonist with optimal pharmacologic and pharmacokinetic properties

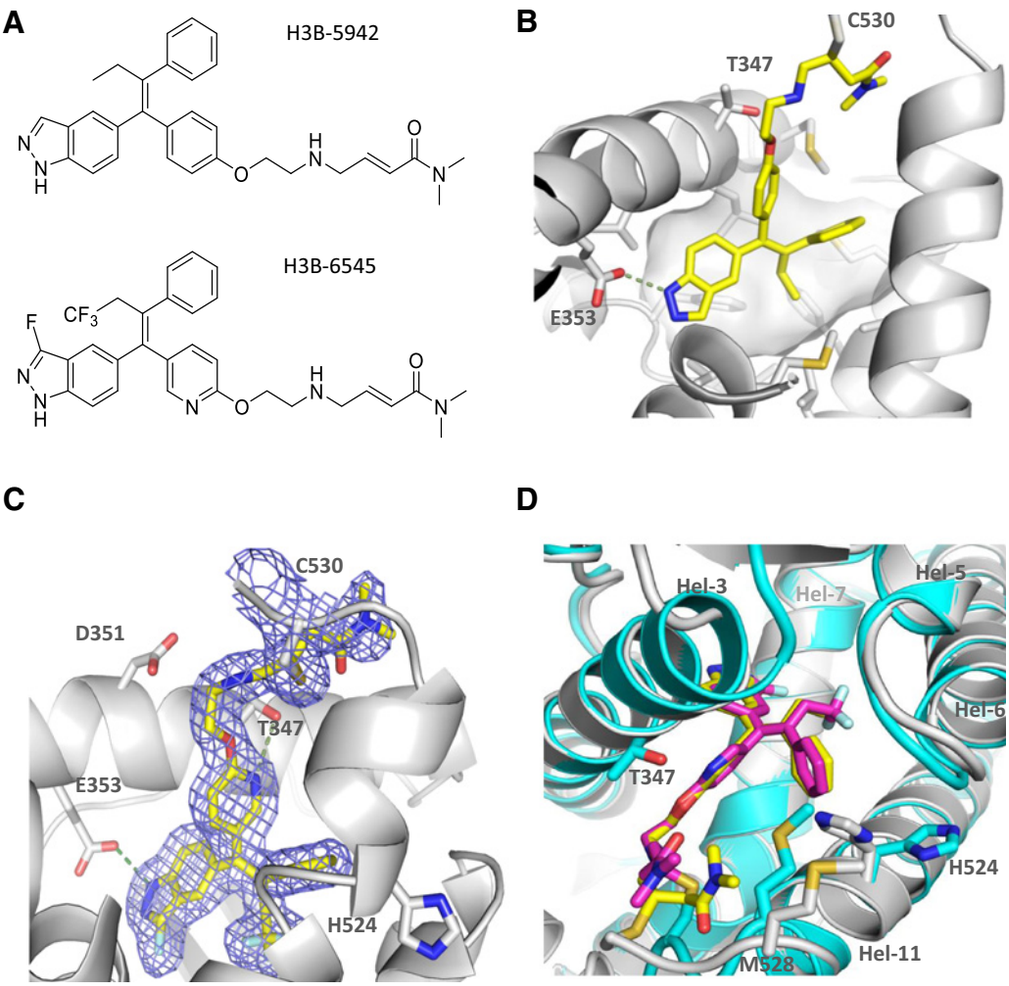

Figure 1.

Identification of H3B-6545, a covalent antagonist with improved potency. **A,** Structural comparison between H3B-5942 and H3B-6545. **B,** X-ray crystal structure of H3B-5942 bound in the ligand-binding domain of $ERα^{Y537S}$. H3B-5942 is rendered as a stick model. The hydrophobic pocket is indicated by the semitransparent surface. H-bonding interactions are rendered as a green dashed line. Other key residues are labeled. **C,** X-ray crystal structure of H3B-6545 bound in the ligand-binding domain of $ERα^{Y537S}$. The protein is rendered as a cartoon model in gray while the ligand is depicted in yellow as a stick model. The 2Fo-Fc electron density map is illustrated as a blue mesh and contoured at 1 sigma. The co-complex structure was crystallized as a dimer in the asymmetric unit. The protein and ligand conformations are identical in chain A and B with the exception of the tail acrylamide of the ligand, which is more flexible. **D,** Comparison of the cocrystal structures of H3B-5942 and H3B-6545 in complex with ERα. The structure of H3B-5942 and H3B-6545 in the cocrystal structure are shown as yellow and magenta stick models, respectively. ERα conformation in chain B of the H3B-6545 cocrystal structure is shown in cyan cartoon model and ERα conformation in chain B of H3B-5942 cocrystal structure shown in gray cartoon model.

Table 1. Comparison of GI_{50} viability and DSF data between H3B-5942 and H3B-6545.

Compounds	Viability (nmol/L)		DSF (°C)	
	WT	Y537S	ΔT_M^{WT}	ΔT_M^{MUT}
4-OHT	1.7 ± 0.4	33.8 ± 20	13.25	13.05
Fulvestrant	0.9 ± 0.2	5.2 ± 3.1	8.74	8.24
Raloxifene	1.0 ± 0.4	26 ± 24.8	12.74	12.01
H3B-5942	1.3 ± 0.6	15.4 ± 8	15.3	15.3
H3B-6545	0.6 ± 0.2	5.3 ± 3.1	16.7	16.6

that would continue to achieve differentiated biological activity over standard-of-care (SoC) therapies but not remain exclusively reliant on covalency for antagonism (24). To achieve this goal, we conducted medicinal chemistry on modifying three areas of the molecule, as exemplified by H3B-5942. The crystal structure of $ER\alpha^{Y537S}$ bound to H3B-5942 (PDB 6CHW) revealed that the core binds in a hydrophobic pocket (**Fig. 1B**). We explored whether modification of the ethyl side chain of the core with small lipophilic substituents might enhance these hydrophobic interactions. In the crystal structure, we also observed an H-bond interaction between the side chain of E353 and the N1 hydrogen of the indazole. Furthermore, we evaluated whether the C ring of the ligand was sufficiently proximal to the hydroxyl side chain of residue T347 to facilitate hydrogen-bonding or electrostatic interaction. We determined that a pyridine substituent at the C ring would achieve this novel H-bond with T347, further enhancing binding affinity while at the same time improving the overall polarity. These structure-based design evaluations ultimately led to incorporation of the trifluoro substitution of the ethyl side chain, 3-fluoro substitution of the indazole, and 3-pyridine substituent at the C ring in the clinical candidate H3B-6545 (**Fig. 1A**, bottom). Taken together, these substitutions afford the best cellular potency while maintaining acceptable physical-chemical properties (**Fig. 1A**; **Table 1**).

Structural characterization of H3B-6545

We determined the crystal structure of $ER\alpha^{Y537S}$ bound to H3B-6545 at 1.85 Å resolution. The crystal structure and intact mass spectrometry confirmed a covalent bond between the acrylamide and C530 (**Fig. 1C**; Supplementary Fig. S1). Overall, the binding mode of H3B-6545 is similar to that of H3B-5942. A structural overlay of the two ligands showed that the indazole ring, ethyl side chain, and B and C rings superimpose closely (**Fig. 1D**). However, the salient interactions between the substituted fluorine atoms of H3B-6545 and Helices-5 and Helices-7 induced conformational changes in ERα. As evident from **Fig. 1D**, two residues on Hel-11, H524, and M528, reorient their side chains; the loop linking Hel-6 to Hel-7 moves closer to Hel-3 and, most notably, the length of Hel-3 extends by one helical turn (S338-S341) in its C-terminal end, placing Hel-3 in direct contact with Hel-5. All these modifications resulted in a more compact structure of the ligand-binding pocket of ERα that would impart stronger interactions with the core scaffold of H3B-6545. Indeed, differential scanning fluorimetry (DSF) confirmed that H3B-6545 bestows greater stabilization to the receptor than H3B-5942 (**Table 1**). Importantly, consistent the selectivity profile previously noted for H3B-5942 (13), H3B-6545 also binds ERα/β with comparable affinities without impacting the function of other closely related nuclear hormone receptors (PRα, PRβ, AR, GR, and MR; Supplementary Table S1).

H3B-6545 is less dependent on covalency for ERα antagonism

To determine the relative contribution of the various unique functional groups of H3B-6545 for driving its interaction with ERα, we synthesized variants of H3B-6545 and H3B-5942 lacking the Michael acceptor, H3B-9709 and H3B-9224, respectively (**Fig. 2A**) (13, 15). Using these tool compounds, we first performed jump dilution experiments to assess whether the additional interactions between ligand and ERα would increase residence time. Here, $ER\alpha^{WT}$ or $ER\alpha^{Y537S}$ was first saturated with ligand, then diluted 20-fold in the presence of an excess of ^{3}H-E2 to titrate the available ERα sites after ligand dissociation over the course of the 22-hour experiment. This allowed us to rank the relative off rates of this set of compounds. We observed the binding of H3B-5942 and H3B-6545 to be irreversible, consistent with their covalent mechanism-of-action (MoA; **Fig. 2B**, left). In the same jump dilution experiments, 4-hydroxytamoxifen (4-OHT), fulvestrant, and H3B-9224 (saturated analog of H3B-5942) were clearly reversible, readily dissociating from ERα after dilution. Remarkably, and in contrast to H3B-9224, the saturated analog of H3B-6545 (H3B-9709) appeared irreversibly bound to both $ER\alpha^{WT}$ and $ER\alpha^{Y537S}$. This result was confirmed using ^{3}H-H3B-9709 jump dilution experiments with unlabeled E2 in which more than 85% of ^{3}H-H3B-9709 remained bound to ERα after dilution (**Fig. 2B**, right). The nature of the interaction between ERα and ^{3}H-H3B-9709 was confirmed to be noncovalent by denaturation of the protein-ligand complex followed by scintillation counting to detect any covalently bound compound. In this experiment, $ER\alpha^{WT}$ or $ER\alpha^{Y537S}$ was almost fully modified by ^{3}H-H3B-6545 within an hour, whereas binding of ^{3}H-H3B-9709 was not observed (**Fig. 2C**). These data collectively suggest that relative to H3B-5942, the modifications of H3B-6545 make it less dependent on covalent engagement for prolonged occupancy on ERα.

Having confirmed reduced dependence of H3B-6545 on C530 for ERα occupancy, we next aimed to assess the impact of covalency on cellular potency. In the cellular setting, both H3B-6545 and H3B-9709 were confirmed to be nondegraders (**Fig. 2D**; Supplementary Fig. S2), had similar global DNA-binding patterns (Supplementary Fig. S3), and nearly identical impact on global gene expression changes (**Fig. 2E**; Supplementary Fig. S4). Importantly, both H3B-6545 and H3B-9709 also similarly suppressed cellular proliferation in $ER\alpha^{WT}$ and $ER\alpha^{Y537S}$ overexpressing MCF7 lines with or without C530 mutations (**Fig. 2F**; Supplementary Table S2), confirming reduced dependence on covalency.

H3B-6545 and H3B-9709 are equipotent across a panel of cell lines expressing various clinically relevant hotspot $ER\alpha^{MUT}$

To confirm the equipotent activity of H3B-6545 and H3B-9709, we broadly profiled the two agents across an expanded panel of MCF7 lines expressing the most frequently occurring ERα hotspot mutations. Consistent with our earlier observation, both compounds demonstrated equal potency across the panel (Supplementary Table S3), suggesting that unlike H3B-5942, H3B-6545 is relatively less dependent on covalency for anti-ERα activity. Interestingly, although H3B-6545 and fulvestrant showed comparable potency in a short-term 6-day proliferation assay in MCF7 engineered lines (Supplementary Table S3), a longer-term confluency assessment revealed that H3B-6545 was capable of maintaining growth suppression longer than fulvestrant at the doses tested in the PDX-derived ST941 cell line (**Fig. 3A**), perhaps owing to its enhanced residence time on ERα.

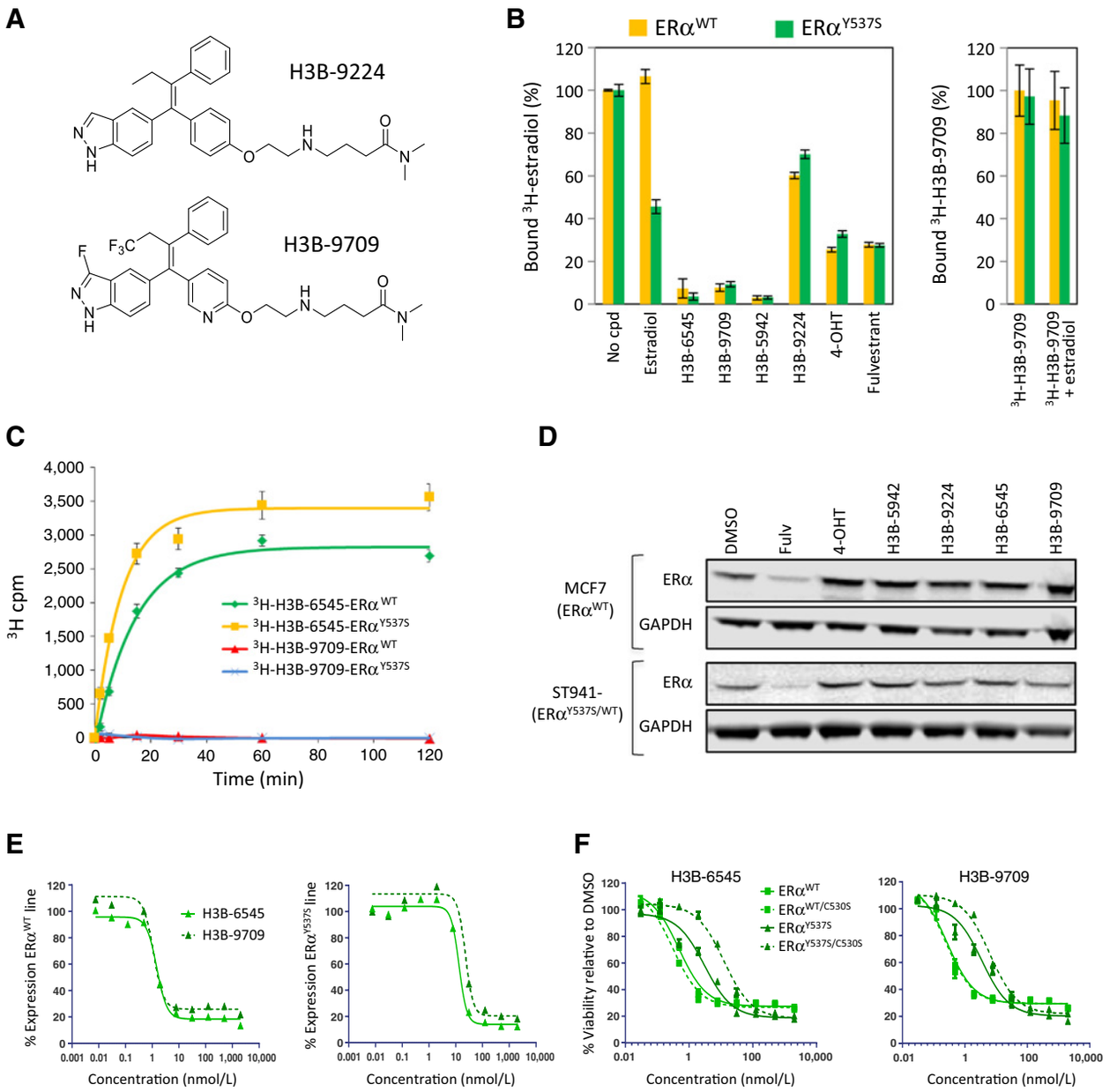

Figure 2.

H3B-6545 is not solely dependent on covalency for anti-ERα activity. **A,** Structures of H3B-9224 and H3B-9709, the saturated analogs of H3B-5942 and H3B-6545, respectively. **B,** Jump dilution experiment to evaluate reversibility of binding of E2 and various inhibitors to ERα^{WT} (yellow bars) and ERα^{Y537S} (green bars). SoC agents 4-OHT and fulvestrant, covalent antagonists H3B-5942 and H3B-6545, and saturated analogs H3B-9224 and H3B-9709 were tested in the assay. Left, ERα was incubated with saturating concentrations of binders followed by 20-fold dilution. A 15-fold final molar excess (7.5 nmol/L) of ^{3}H-E2:binder was then used to titrate the number of ERα sites that were no longer bound to the initial binder after dilution. The assay was performed as described previously (13). Right, The assay was performed similarly except that saturating concentrations of ^{3}H-H3B-9709 were used followed by dilution and incubation with an excess of unlabeled E2 to titrate unbound ERα. **C,** Kinetics of covalent engagement monitored by ^{3}H-protein labeling for ERα^{WT} and ERα^{Y537S}. ERα was incubated with ^{3}H-H3B-6545 and ^{3}H-H3B-9709 at room temperature for various times followed by protein denaturation and precipitation. The protein pellet was resolubilized and ^{3}H-labeling was quantified by liquid scintillation counting. k_{obs} values of $(1.2 \pm 0.2) \times 10^{-3}$ second^{-1} and $(1.7 \pm 0.3) \times 10^{-3}$ second^{-1} were obtained for the labeling of ERα^{WT} and ERα^{Y537S} by ^{3}H-H3B-6545, respectively. **D,** Western blot analysis of ERα expression following a 24-hour treatment with the indicated compounds at 100 nmol/L in the MCF7 parental line (MCF7-Parental) and the ST941 PDX model derived cell line (PDX-ERα$^{Y537S/WT}$). GAPDH was used as loading control. **E,** Representative plots showing dose-dependent suppression in *GREB1* expression in ERα^{WT} (left) and ERα^{Y537S} (right) expressing MCF7 cells following a 6-day treatment with H3B-6545 (green solid) and H3B-9709 (green dotted). **F,** Representative graphs showing a dose-dependent decrease in proliferation of ERα^{WT} and ERα^{Y537S} MCF7 overexpressing lines with or without C530S mutation in ERα following 6-day treatment with H3B-6545 (left) and H3B-9709 (right).

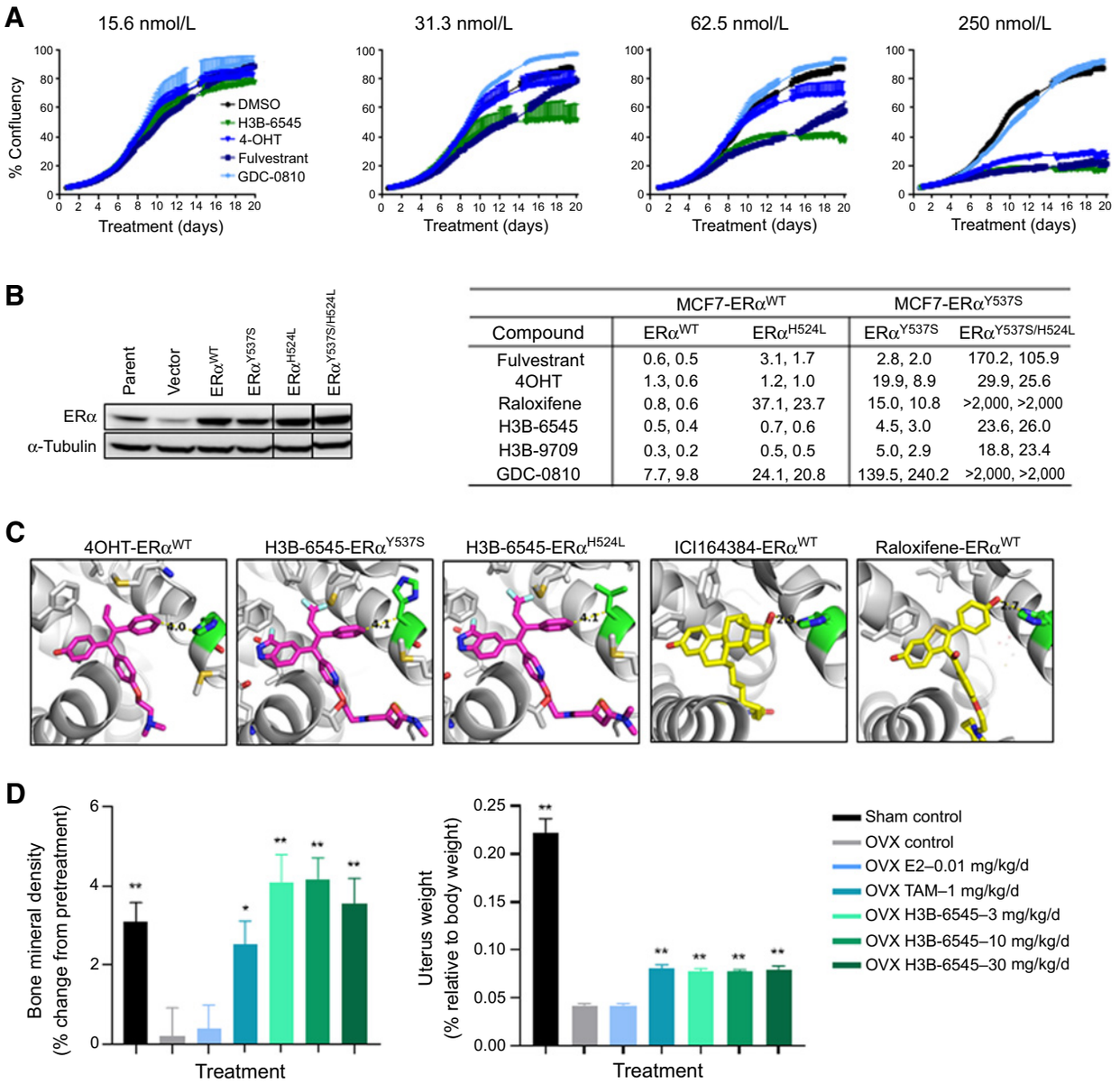

Compound	MCF7-ERαWT		MCF7-ERαY537S	
	ERαWT	ERαH524L	ERαY537S	ERαY537S/H524L
Fulvestrant	0.6, 0.5	3.1, 1.7	2.8, 2.0	170.2, 105.9
4OHT	1.3, 0.6	1.2, 1.0	19.9, 8.9	29.9, 25.6
Raloxifene	0.8, 0.6	37.1, 23.7	15.0, 10.8	>2,000, >2,000
H3B-6545	0.5, 0.4	0.7, 0.6	4.5, 3.0	23.6, 26.0
H3B-9709	0.3, 0.2	0.5, 0.5	5.0, 2.9	18.8, 23.4
GDC-0810	7.7, 9.8	24.1, 20.8	139.5, 240.2	>2,000, >2,000

Figure 3.

H3B-6545 demonstrates potent antagonist activity across a panel of ERα$^{WT/MUT}$ cell lines and SERM activity in bone and uterine tissues. **A,** IncuCyte-based confluency assessment of ST941 cells following treatment with H3B-6545, 4-OHT, fulvestrant, and GDC-0810 at the indicated concentrations. Data represent the mean confluence ± SD. **B,** Western blot analysis for ERα confirming H524 L overexpression in MCF7 lines overexpressing ERα^{WT} or ERα^{Y537S} with α-tubulin as a loading control (left) and table showing antiproliferative activity (GI_{50}) for indicated compounds in ERα^{WT} and ERα^{Y537S} overexpressing MCF7 cells with or without H524 L *ESR1* mutation (right). **C,** X-ray cocrystal structures of 4-OHT (pdb: 3ERT) in complex with ERα, H3B-6545 (pdb: 6OWC) in complex with ERα^{Y537S}, H3B-6545 (homology model) in complex with ERα^{H524L}, fulvestrant analog ICI164384 (pdb: 1HJ1) and raloxifene (pdb: 1ERR) (right) in complex with ERα^{WT}. **D,** Left, femur global BMD measured by DXA in rats that underwent sham or OVX surgery followed by daily treatment with 17β-estradiol (E2, 0.01 mg/kg/day), tamoxifen (TAM, 1 mg/kg/day), and H3B-6545 (3, 10, and 30 mg/kg/day) for 6 weeks. Data represent the percentage of change at week 5/6 after treatment compared with pretreatment (mean ± SEM, $N = 20$). *, $P < 0.05$; **, $P < 0.01$ versus OVX control. **D,** (Right), the relative uterus weight (vs BW) in rats that underwent sham or OVX surgery followed by daily treatment with E2, TAM, and H3B-6545 for 6 weeks. Data represent the mean ± SEM ($N = 20$). *, $P < 0.05$; **, $P < 0.01$ versus OVX control.

H3B-6545 demonstrates potency against the clinically relevant ERα^{H524L}

On the basis of the data presented, it is likely that reduced dependence on covalency can be attributed to additional noncovalent interactions by the abovementioned functionalities. However, we could not rule out the involvement of the positional changes observed in H524 and M528 following binding of H3B-6545 relative to H3B-5942 (**Fig. 1D**). Previous studies have implicated the role of H524 in binding to E2, fulvestrant, and raloxifene through formation of a key H-bond interaction with the ligands (25, 26), and interestingly,

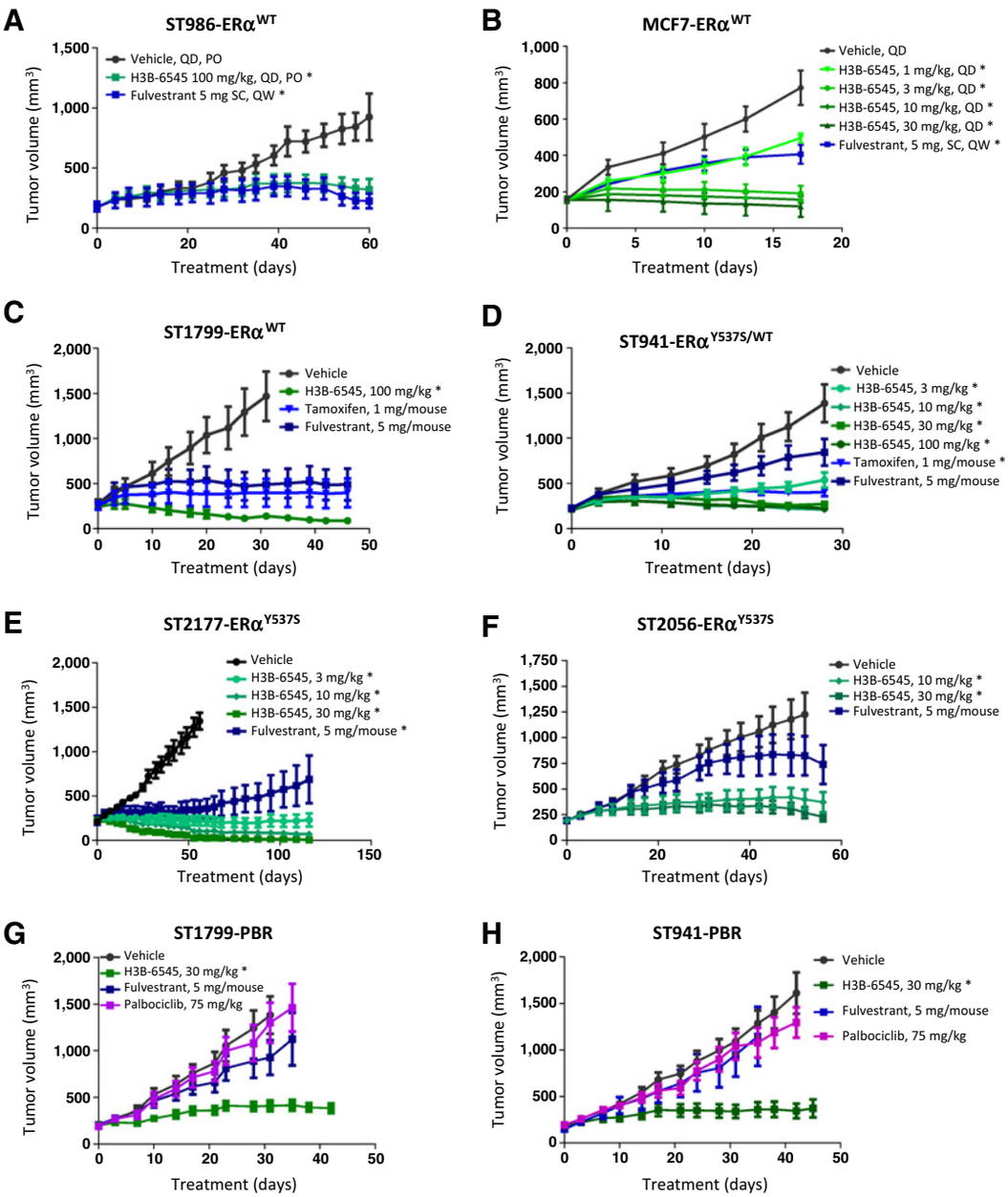

Figure 4.

H3B-6545 demonstrates single-agent antitumor activity in ERα^{WT} and ERα^{MUT} xenograft models. **A,** Antitumor activity of H3B-6545 compared with fulvestrant in the ERα^{WT} ST986 PDX model. H3B-6545 was administered orally once daily at 100 mg/kg in mice bearing xenograft tumors representing ERα^{WT} breast cancer. Fulvestrant was dosed subcutaneous once weekly at 5 mg/mouse. Data represent the mean tumor volume ± SEM ($N = 6$ for H3B-6545 treatment arm, $N = 6$ for all other treatments). Statistical significance assessed on day 60. **B,** Antitumor activity of H3B-6545 compared to fulvestrant in the ERα^{WT} MCF7 CDX model. H3B-6545 was administered orally once daily at 1, 3, 10, and 30 mg/kg whereas fulvestrant was dosed subcutaneously once weekly at 5 mg/mouse. Data represent the mean tumor volume ± SEM ($N = 6$). Statistical significance assessed on day 17. **C,** Antitumor activity of H3B-6545 compared with tamoxifen and fulvestrant in the ERα^{WT} ST1799 PDX model. H3B-6545 was administered orally once daily at 100 mg/kg in mice bearing xenograft tumors representing ERα^{WT} breast cancer. Tamoxifen was dosed subcutaneously three times a week at 1 mg/mouse whereas fulvestrant was dosed subcutaneously once weekly at 5 mg/mouse. Data represent the mean tumor volume ± SEM ($N = 5$ for H3B-6545 treatment arm, $N = 6$ for all other treatments). Statistical significance assessed on day 31. **D,** Antitumor activity of H3B-6545 compared with tamoxifen and fulvestrant in the ERα$^{Y537S/WT}$ ST941 PDX model. H3B-6545 was administered orally once daily at 3, 10, 30, and 100 mg/kg in mice bearing xenograft tumors representing ERα$^{Y537S/WT}$ breast cancer. Tamoxifen was dosed subcutaneously three times a week at 1 mg/mouse whereas fulvestrant was dosed subcutaneously once weekly at 5 mg/mouse. Data represent the mean tumor volume ± SEM ($N = 8$ for vehicle, tamoxifen and fulvestrant arms, $N = 6$ for all H3B-6545 treatments). Statistical significance assessed on day 28. **E,** Antitumor activity of H3B-6545 compared with fulvestrant in the ERα^{Y537S} ST2177 PDX model. H3B-6545 was administered orally once daily at 3, 10, and 30 mg/kg in mice bearing xenograft tumors. Fulvestrant was dosed subcutaneously once weekly at 5 mg/mouse. Data represent the mean tumor volume ± SEM ($N = 6$ for fulvestrant, $N = 7$ for all other treatments). (*Continued on the following page.*)

H524L/Y mutations have been noted at low frequency in relapsed/metastatic breast cancer (27). We confirmed the enrichment of H524L/Y in an independent cohort of metastatic breast cancer samples relative to local breast cancer samples. H524L/Y mutations were not significantly represented in The Cancer Genome Atlas primary untreated (0 of 791) or Foundation Medicine (FMI) local samples from breast biopsies (0 of 620). However, there were 20 cases noted from FMI metastatic biopsy sites that harbored *ESR1* H524L/Y mutations (20 of 4,201; Supplementary Table S4). This pattern was similar to *ESR1* hotspot alterations at codons 380 and 536–538, suggesting that H524L/Y recurrent mutations in ERα may affect disease progression and/or response to current antiestrogens. To assess whether H524 mutations might impact H3B-6545 activity, we tested the potency of H3B-6545 and H3B-9709 in MCF7 lines engineered to overexpress $ER\alpha^{WT}$ or $ER\alpha^{Y537S}$ with or without the clinically relevant H524L mutation (**Fig. 3B**, left). Convincingly, H3B-6545 showed comparable activity across the various cell lines suggesting that H524 is likely not a critical residue for activity. A similar observation was also made for H3B-9709 and 4-OHT. In contrast, fulvestrant and raloxifene showed greater dependence on H524 as a >30-fold drop in potency was observed when mutated in the $ER\alpha^{Y537S}$ setting (**Fig. 3B**, right). Whereas crystal structures for both the fulvestrant analog ICI 164384 (pdb: IHJ1) and raloxifene (pdb: 1ERR) suggest the formation of strong hydrogen bonds with H524, corresponding crystal structures for 4-OHT (pdb: 3ERT) and H3B-6545 (pdb: 6OWC) indicate only a weak van der Waals contact with H524, potentially explaining why the latter ligands remain effective in the H524L setting (**Fig. 3C**).

H3B-6545 presents tissue- and context-dependent SERM activity

Having demonstrated significant antagonist activity of H3B-6545 across a large panel of ERα wild-type and variant lines, we next aimed to assess SERM activity of H3B-6545 in the cancer and normal tissue settings. We first analyzed the effect of various compounds on the expression of a subset of the breast cancer–specific SERM discriminatory genes following treatment of MCF7 cells cultured in the absence of E2 (4, 28). Relative to 4-OHT, H3B-6545 showed only a minor reduction in agonist activity for the majority of the genes profiled. Interestingly, although H3B-9709 shows comparable antagonism potency as H3B-6545 in the MCF7 line cultured in the presence of E2 (Supplementary Table S3), it presented modestly greater agonist activity relative to H3B-6545 for many of the genes profiled in the absence of E2 (Supplementary Fig. S5A). Interestingly, and consistent with the differential SERM activity noted in the MCF7 cells, we observed a similar trend in the endometrial carcinoma setting. Whereas 4-OHT and H3B-9709 robustly enhanced proliferation of the Ishikawa endometrial carcinoma cell line, H3B-6545 showed relatively reduced agonist activity under the culture conditions tested (Supplementary Fig. S5B). These data in aggregate imply that covalent engagement with C530 of ERα in the cancer setting may modestly blunt SERM activity relative to 4-OHT and non-covalent variants, although more data with additional analogs are needed to strengthen this observation.

Consistent with the cancer cell line setting, H3B-6545 also demonstrated SERM activity in normal bone and endometrial tissues. As expected, OVX of 6-month-old female rats significantly reduced bone density (7% of sham control; **Fig. 3D**, left) and uterine weights (**Fig. 3D**, right), whereas tamoxifen treatment restored bone density loss to 82% of sham control (**Fig. 3D**, left) and enhanced uterine weights to 82%–93% greater than OVX controls. Consistent with tamoxifen, H3B-6545 treatment also reversed OVX-induced bone density loss (133%, 135%, and 114% of sham control at 3, 10, and 30 mg/kg/day, respectively), and increased uterus weights in a dose-independent manner to levels observed for tamoxifen. Collectively, these data imply tissue- and context-dependent differential SERM activity for H3B-6545.

H3B-6545 has potent antitumor activity in $ER\alpha^{WT}$ and $ER\alpha^{MUT}$ breast tumor models

Having confirmed robust cellular potency of H3B-6545 and H3B-9709 *in vitro*, we next aimed to assess antitumor activity across various cell line-derived xenograft (CDX) and PDX tumor models harboring $ER\alpha^{WT}$ or $ER\alpha^{MUT}$. Analysis of the pharmacokinetic profile of both agents in mice and rats revealed favorable properties for H3B-6545 in both species. However, H3B-9709 demonstrated a less than desirable profile with significantly reduced overall exposure (∼30-fold reduction relative to H3B-6545) and enhanced volume of distribution (Vss = 9.7) in rats (Supplementary Table S5). In aggregate, the favorable pharmacokinetic profile of H3B-6545 and reduced *in vitro* SERM activity (Supplementary Fig. S5) contributed to the selection of the covalent agent for further investigation.

We next aimed to determine the pharamacokinetic/pharmacodynamic relationship for H3B-6545 in both $ER\alpha^{WT}$ and $ER\alpha^{Y537S/WT}$ models. In the $ER\alpha^{WT}$ MCF7 tumor model, H3B-6545 dosed once orally at 1–30 mg/kg showed a dose-proportional increase in plasma and tumor exposure, and a concomitant dose-proportional decrease in expression of ERα target genes, *PGR* and *GREB1*. Notably, a single dose of H3B-6545 at 30 mg/kg was sufficient to suppress both *PGR* and *GREB1* for up to 72 hours postdose (Supplementary Fig. S6). Five daily oral doses of H3B-6545 at 3–100 mg/kg in the $ER\alpha^{Y537S/WT}$ ST941 model suppressed the ERα target PR and the proliferation marker Ki67 in a dose-proportional manner with 30 and 100 mg/kg doses maintaining suppression for up to 72 hours after last dose. Importantly, ERα activity was suppressed without any impact on ERα levels, consistent with the MoA of H3B-6545 (Supplementary Fig. S7).

Having determined that once daily dosing of H3B-6545 would maintain pathway suppression, we next evaluated efficacy across three $ER\alpha^{WT}$ CDX/PDX models. In the ST986 PDX model, once weekly subcutaneous dosing of fulvestrant at 5 mg/mouse or daily oral dosing of H3B-6545 at 100 mg/kg resulted in near stasis (**Fig. 4A**). However, whereas H3B-6545 and fulvestrant showed comparable efficacy in the ST986 model, H3B-6545 demonstrated superiority in the $ER\alpha^{WT}$

(*Continued.*) Statistical significance assessed on day 56. **F,** Antitumor activity of H3B-6545 compared with fulvestrant in the $ER\alpha^{Y537S}$ ST2056 PDX model. H3B-6545 was administered orally once daily at 100 mg/kg whereas fulvestrant was dosed subcutaneously once weekly at 5 mg/mouse in mice bearing xenograft tumors. Data represent the mean tumor volume ± SEM ($N = 8$). Statistical significance assessed on day 22. **G,** Antitumor activity of H3B-6545 in the palbociclib-resistant ST1799-PBR model. H3B-6545 was administered orally once daily at 3, 10, and 30 mg/kg and palbociclib was administered orally once daily at 75 mg/kg. Data represent the mean tumor volume ± SEM ($N = 7$ for vehicle arm, $N = 8$ for all other treatments). Statistical significance assessed on day 46. **H,** Antitumor activity of H3B-6545 in the palbociclib-resistant ST941-PBR model. H3B-6545 was administered orally once daily at 30 mg/kg, palbociclib was administered orally once daily at 50 mg/kg, and fulvestrant was administered subcutaneously once weekly at 5 mg/mouse. Data represent the mean tumor volume ± SEM ($N = 6$). Statistical significance assessed on day 42. *, $P < 0.05$ versus vehicle control (multiple unpaired t tests with significance determined using the Holm-Sidak method). All doses and regimens were well tolerated.

MCF7 and ST1799 CDX and PDX models, respectively. In the MCF7 model, whereas fulvestrant treatment resulted in tumor growth inhibition (TGI) of 48%, H3B-6545 at 3 mg/kg suppressed tumor growth by 75% (**Fig. 4B**). In contrast to the stasis observed in the MCF7 model, daily oral dosing of H3B-6545 at 100 mg/kg resulted in significant regressions in the ST1799 model, superior to the stasis observed with the SoC tamoxifen or fulvestrant (**Fig. 4C**). In a subsequent study, we confirmed that regressions could be achieved at H3B-6545 doses as low as 3 mg/kg in the ST1799 model (Supplementary Fig. S8A).

Having demonstrated antitumor activity of H3B-6545 across multiple ERα^{WT} CDX/PDX models, we next evaluated H3B-6545 activity across three ERα^{Y537S} PDX models. Oral once daily administration of 3, 10, 30, and 100 mg/kg H3B-6545 in the ERα$^{Y537S/WT}$ ST941 model resulted in dose-dependent inhibition of tumor growth (TGI on day 28 of 61%, 85%, 81%, and 85%, respectively; **Fig. 4D**), and dose-dependent decrease in PR and Ki67 in endpoint tumors, with near maximal suppression in pharmacodynamic expression observed at 10 mg/kg, the saturating efficacious dose in this model (Supplementary Fig. S8B). Although tamoxifen and fulvestrant also inhibited tumor growth (TGI of 71% and 39%, respectively), H3B-6545 demonstrated superior activity at the level of both pharmacodynamic modulation and antitumor activity (**Fig. 4D**; Supplementary Fig. S8B). Consistent with the significant antitumor activity in the ST941 model, H3B-6545 also demonstrated superior activity over SoC in two additional mutant PDX tumor models harboring the ERα^{Y537S} mutation. Whereas subcutaneous dosing of fulvestrant inhibited tumor growth in the ST2177 model, resulting in near stasis (TGI on day 56 of 74%), daily oral dosing of H3B-6545 at 3–30 mg/kg led to a dose-dependent inhibition in tumor growth (TGI on day 56 of 87%, 94%, and 98%), with regressions observed at 10–30 mg/kg (**Fig. 4E**). Consistent with the superior activity observed in both the ST941 and ST2177 PDX models, H3B-6545 at 10 and 30 mg/kg also demonstrated superior anti-tumor activity over fulvestrant in the ERα^{Y537S} ST2056 PDX model (**Fig. 4F**). Collectively, *in vivo* profiling confirmed H3B-6545 has potent single-agent antitumor activity in both the ERα^{WT} and ERα^{MUT} setting at well-tolerated doses.

As the ERα^{WT} and ERα^{MUT} models described above were derived from patients not previously treated with CDK4/6 inhibitors, a therapy approved first line in combination with endocrine therapies, we next aimed to assess whether H3B-6545 could demonstrate single-agent efficacy in the palbociclib-resistant ST1799-PBR and ST941-PBR models, which were derived following continuous exposure to palbociclib *in vivo*. Whereas these tumor models are completely resistant to palbociclib and fulvestrant treatments, significant antitumor activity was achieved following single-agent H3B-6545 treatment (**Fig. 4G** and **H**). In summary, the encouraging single-agent activity of H3B-6545 across a range of animal models described above suggests that H3B-6545 may be effective in both palbociclib-naïve and palbociclib-resistant patients with ER^{+} breast cancer in the clinic.

Discussion

Previously, we showed H3B-5942 is highly dependent on covalent engagement with C530 residue for antagonism, as mutation of this residue or elimination of the Michael acceptor in H3B-5942 led to a remarkable decrease in potency. Although some mutations in ERα can compromise or enhance basal or E2-induced activity of ERα, several laboratories have shown that C530A/H/L/R/F/Y/V/S mutations do not significantly impact the E2-induced transactivation activity of the protein (13, 23), suggesting that these mutations could be selected by the tumor to evade activity. In light of this potential liability, we aimed to develop an improved antagonist that would continue to engage selectively with C530 to promote differentiated mechanism of action and biology but not remain critically dependent on this interaction for ERα antagonism activity. Using the structure of ERα bound to H3B-5942, we explored whether regions of the core could benefit from additional, stronger interactions to enhance residence time on ERα and thus, reduce dependence on covalency for ERα occupancy. Our structure-based drug design efforts led to the identification of clinical candidate H3B-6545. On the basis of the ERα-H3B-6545 cocrystal structure (**Fig. 1C**), we noted a more compact structure of the ligand-binding pocket relative to the ERα-H3B-5942 structure, suggesting that the stronger network of interactions might be playing a role in addition to covalent engagement for H3B-6545. Besides the potential importance of additional hydrophobic and hydrophilic interactions, we also tested the functional role of H524 on H3B-6545 potency as its position varied between the H3B-5942 and H3B-6545 cocrystal structures with ERα. Interestingly, we found that whereas the H524 L mutation did not significantly compromise H3B-6545 activity, the mutation did blunt the activity of fulvestrant and raloxifene. Although H524 has previously been shown to be critical for E2-induced transactivation (25, 26), its potential importance in fulvestrant/raloxifene potency is less appreciated. A recent study by Chung and colleagues (2017) (27) reported H524L/Y *ESR1* variants by analyzing ctDNA from patients with breast cancer bearing metastases. Independently, we also confirmed these recurrent mutations are enriched at low frequencies in the metastatic setting, suggesting they may functionally promote disease progression and/or resistance to endocrine therapies. It is interesting to note that although *in vitro* data supports *ESR1*-H524L mutation as a potential resistance mechanism to fulvestrant, this mutation is rarely observed in the clinic. One possible explaination for this apparent *in vitro*-clinical disconnect may be the suboptimal selection pressure achieved in the tumor setting due to the low exposure of fulvestrant noted in the clinic. It will be interesting to continue to monitor the genomic landscape as more potent ERα antagonists with improved pharmacokinetic properties are introduced into the clinic, particularly for those agents that derive potency from H524 engagement.

It is now becoming evident that the mutational landscape of *ESR1* in refractory metastases is complex, with several lower frequency mutations being enriched in the metastatic setting (naïve or treatment-related) for which the function is unclear (29). It is conceivable that like H524L/Y, other low-frequency mutations may similarly impact interactions with ligands to drive resistance to existing therapies or more generically influence ERα conformation/function to influence disease progression/resistance. Thus, interrogation of the functional role of these low-frequency mutations is warranted to expand our understanding of the structure/function relationships and the overarching mechanisms that promote resistance to endocrine therapies.

In-house and literature data strongly suggest that Y537S mutation in ERα is the most constitutively activating and, likely as a consequence, the most potent driver of resistance to various endocrine therapies. On the basis of the encouraging preclinical activity of H3B-6545 in PDX models bearing the Y537S allele, H3B-6545 clinical activity is being investigated in patients with pretreated ER^{+}, HER2^{-} metastatic breast cancer, including those bearing Y537S (NCT03250676). Consistent with the preclinical studies, H3B-6545 is demonstrating preliminary single-agent antitumor activity in both the WT and Y537S settings, including patients with high *ESR1* Y537S MAF (30–32), suggesting that H3B-6545 may have the potential to therapeutically overcome resistance driven by the emergence of the Y537S mutation in ERα.

Although there have been significant efforts to develop potent SERDs with pure antagonist activities, development of an ER antagonist with a favorable SERM profile may also be considered. Here we demonstrated that H3B-6545 and tamoxifen treatments significantly reduced bone loss in aged rats following ovariectomy, implying that H3B-6545 treatment, similar to tamoxifen in the clinic, may not accelerate bone loss which has been noted for aromatase inhibitors following adjuvant treatment in the clinic (33). The impact of long-term treatment with novel SERDs has yet to be assessed.

Consistent with the SERM activity noted in bone, we also note partial agonistic activity for tamoxifen and H3B-6545 in the normal rat uterus following a 6-week treatment period. Although both compounds similarly promoted epithelial hypertrophy and enhanced uterine weights at the doses tested, it is unclear how the intrinsic agonism of these compounds compare due to differential exposures of the compounds in the study. Collectively, in light of these data, the impact of H3B-6545 treatment on bone health and endometrial thickening/uterine volume is currently being monitored in the phase I/II trial.

Authors' Disclosures

Z.J. Wu reports other support from H3B outside the submitted work. L.A. Albacker reports employment by Foundation Medicine and stockholder of Roche AG. M.-H. Hao reports a patent for US 9796683 issued and a patent for US 10851065 issued. M. Montesion reports personal fees from Foundation Medicine and Roche Holding AG outside the submitted work. K. Murugesan reports other support from Foundation Medicine Inc, Cambridge, MA and Roche outside the submitted work; and Patents, Royalties, Other Intellectual Property: Antibiotic resistance causation identification (US10629291B2) granted with Koninklijke Philips NV, Analytic prediction of antibiotic susceptibility (US20190279738A1) filed with Koninklijke Philips NV, Methodology for measuring the quality of phylogenetic and transmission trees and for merging trees (US16/760,213) filed with Koninklijke Philips NV, Methods and devices for characterizing and treating combined hepatocellular cholangiocarcinoma, with Foundation Medicine Inc. T. Sahmoud reports personal fees from H3 Biomedicine during the conduct of the study; personal fees from Context Therapeutics outside the submitted work. S. Prajapati reports a patent for US 9796683 B2 issued and a patent for US 2018/0141913 A1 pending. P. Zhu is a full-time employee of H3 Biomedicine, Inc. M. Korpal reports a patent for US 9,796,683, B2 Example (60) issued. No disclosures were reported by the other authors.

Authors' Contributions

C. Furman: Conceptualization, data curation, supervision, validation, investigation, methodology, writing–original draft, writing–review and editing. **X. Puyang:** Conceptualization, data curation, validation, investigation, methodology. **Z. Zhang:** Data curation, formal analysis, validation, writing–original draft, writing–review and editing. **Z.J. Wu:** Data curation, formal analysis. **D. Banka:** Validation, investigation. **K.B. Aithal:** Investigation. **L.A. Albacker:** Data curation, formal analysis. **M.-H. Hao:** Data curation, formal analysis. **S. Irwin:** Validation, investigation. **A. Kim:** Formal analysis, investigation. **M. Montesion:** Data curation, formal analysis. **A.D. Moriarty:** Investigation. **K. Murugesan:** Data curation, formal analysis. **T.-V. Nguyen:** Investigation. **V. Rimkunas:** Formal analysis, validation, investigation. **T. Sahmoud:** Project administration, writing–review and editing. **M.J. Wick:** Methodology, project administration. **S. Yao:** Investigation. **X. Zhang:** Formal analysis. **H. Zeng:** Investigation. **F.H. Vaillancourt:** Supervision, writing–original draft. **D.M. Bolduc:** Investigation, writing–original draft. **N. Larsen:** Supervision. **G.Z. Zheng:** Conceptualization, supervision. **S. Prajapati:** Conceptualization, investigation, writing–original draft. **P. Zhu:** Conceptualization, supervision, writing–review and editing. **M. Korpal:** Conceptualization, data curation, formal analysis, supervision, validation, investigation, writing–original draft, writing–review and editing.

Acknowledgments

We thank our past H3 Biomedicine colleagues Subhasree Das, Jaya J. Joshi, Morgan O'Shea, Lorna S. Mitchell, Nathalie Rioux, Joanne Schindler, Peter G. Smith, Michael Thomas, John Wang, Lihua Yu, and Markus Warmuth for supporting the program. We also thank our colleagues Sujatha Rajagopalan and Sasirekha Sivakumar from Aurigene Discovery Technologies Ltd for performing the MCF7 studies.

The costs of publication of this article were defrayed in part by the payment of page charges. This article must therefore be hereby marked *advertisement* in accordance with 18 U.S.C. Section 1734 solely to indicate this fact.

Received April 28, 2021; revised August 19, 2021; accepted March 18, 2022; published first March 31, 2022.

References

1. Li S, Shen D, Shao J, Crowder R, Liu W, Prat A, et al. Endocrine-therapy-resistant ESR1 variants revealed by genomic characterization of breast-cancer-derived xenografts. Cell Rep 2013;4:1116–30.
2. Robinson DR, Wu Y-M, Vats P, Su F, Lonigro RJ, Cao X, et al. Activating ESR1 mutations in hormone-resistant metastatic breast cancer. Nat Genet 2013;45:1446–51.
3. Toy W, Shen Y, Won H, Green B, Sakr RA, Will M, et al. ESR1 ligand-binding domain mutations in hormone-resistant breast cancer. Nat Genet 2013;45:1439–45.
4. Joseph JD, Darimont B, Zhou W, Arrazate A, Young A, Ingalla E, et al. The selective estrogen receptor downregulator GDC-0810 is efficacious in diverse models of ER+ breast cancer. eLife 2016;5:e15828.
5. Weir HM, Bradbury RH, Lawson M, Rabow AA, Buttar D, Callis RJ, et al. AZD9496: an oral estrogen receptor inhibitor that blocks the growth of ER-positive and ESR1-mutant breast tumors in preclinical models. Cancer Res 2016;76:3307–18.
6. Bihani T, Patel HK, Arlt H, Tao N, Jiang H, Brown JL, et al. Elacestrant (RAD1901), a selective estrogen receptor degrader (SERD), has antitumor activity in multiple ER(+) breast cancer patient-derived xenograft models. Clin Cancer Res 2017;23:4793–804.
7. Guan J, Zhou W, Hafner M, Blake RA, Chalouni C, Chen IP, et al. Therapeutic ligands antagonize estrogen receptor function by impairing its mobility. Cell 2019;178:949–63.
8. El-Ahmad Y, Tabart M, Halley F, Certal V, Thompson F, Filoche-Romme B, et al. Discovery of 6-(2,4-Dichlorophenyl)-5-[4-[(3S)-1-(3-fluoropropyl)pyrrolidin-3-yl]oxyphenyl]-8, 9-dihydro-7H-benzo[7]annulene-2-carboxylic acid (SAR439859), a potent and selective estrogen receptor degrader (SERD) for the treatment of estrogen-receptor-positive breast cancer. J Med Chem 2020;63:512–28.
9. Kaklamani V, Bardia A, Wilks S, Weise A, Richards D, Harb W, et al. Final analysis of phase 1 study of elacestrant (RAD1901), a novel selective estrogen receptor degrader (SERD), in estrogen receptor positive (ER+), human epidermal growth factor receptor 2 negative (HER2-) advanced breast cancer. Cancer Res 2020;80:PD7-07.
10. Lim E, Jhaveri K, Perez Fidalgo JA, Bellet M, Boni V, Perez Garcia JM, et al. A phase 1B study to evaluate the oral selective estrogen receptor degrader GDC-9545 alone or combined with palbociclib in metastatic ER-positive HER2-negative breast cancer. J Clin Oncol 38:15s, 2020 (suppl; abstr 1023).
11. Linden HM, Campone M, Bardia A, Ulaner GA, Gosselin A, Doroumian S, et al. A phase 1/2 study of amcenestrant (SAR439859), an oral selective estrogen receptor (ER) degrader (SERD), as monotherapy and in combination with other anti-cancer therapies in postmenopausal women with ER-positive (ER+) /human epidermal growth factor receptor 2-negative (HER2−) metastatic breast cancer (mBC): AMEERA-1; 2020.
12. Baird R, Oliveira M, Ciruelos EM, Patel MR, Benejo de las Heras B, Ruiz-Borrego M, et al. Updated data from SERNA-1: a phase 1 dose escalation and expansion study of the next generation oral SERD AZD9833 as a monotherapy and in combinatin with palbociclib, in women with ER-positive, HER2-negative advanced breast cancer; 2020.
13. Puyang X, Furman C, Zheng GZ, Wu ZJ, Banka D, Aithal K, et al. Discovery of selective estrogen receptor covalent antagonists for the treatment of ERalpha (WT) and ERalpha(MUT) breast cancer. Cancer Discov 2018;8:1176–93.

14. Bock M, Hao M-H, Korpal M, Nyavanandi VK, Puyang X, Samajdar S, et al. Tetrasubstituted alkene compounds and their use. United States: Eisai R&D Management Co., LTD., Tokyo (JP); 2017.
15. Bock M, Hao M-H, Korpal M, Nyavanandi VK, Puyang X, Samajdar S, et al. Tetrasubsitituted alkene compounds and their use. United States: Eisai R&D Management Col, LTD., Tokyo (JP); 2018.
16. Coser KR, Chesnes J, Hur J, Ray S, Isselbacher KJ, Shioda T. Global analysis of ligand sensitivity of estrogen inducible and suppressible genes in MCF7/BUS breast cancer cells by DNA microarray. Proc Natl Acad Sci U S A 2003;100: 13994–9.
17. Norman RA, Schott A-K, Andrews DM, Breed J, Foote KM, Garner AP, et al. Protein-ligand crystal structures can guide the design of selective inhibitors of the FGFR tyrosine kinase. J Med Chem 2012;55:5003–12.
18. Vagin A, Teplyakov A. Molecular replacement with MOLREP. Acta Crystallogr D Biol Crystallogr 2010;66:22–25.
19. Murshudov GN, Vagin AA, Dodson EJ. Refinement of macromolecular structures by the maximum-likelihood method. Acta Crystallogr D Biol Crystallogr 1997;53:240–55.
20. Bray NL, Pimentel H, Melsted P, Pachter L. Near-optimal probabilistic RNA-seq quantification. Nat Biotechnol 2016;34:525–7.
21. Robinson MD, Mccarthy DJ, Smyth GK. edgeR: a Bioconductor package for differential expression analysis of digital gene expression data. Bioinformatics 2010;26:139–40.
22. Law CW, Chen Y, Shi W, Smyth GK. voom: Precision weights unlock linear model analysis tools for RNA-seq read counts. Genome Biol 2014;15:R29.
23. Reese JC, Katzenellenbogen BS. Mutagenesis of cysteines in the hormone binding domain of the human estrogen receptor. Alterations in binding and transcriptional activation by covalently and reversibly attaching ligands. J Biol Chem 1991;266:10880–7.
24. Furman C, Hao M-H, Prajapati S, Reynolds D, Rimkunas V, Zheng GZ, et al. Estrogen receptor covalent antagonists: the best is yet to come. Cancer Res 2019; 79:1740–5.
25. Ekena K, Weis KE, Katzenellenbogen JA, Katzenellenbogen BS. Different residues of the human estrogen receptor are involved in the recognition of structurally diverse estrogens and antiestrogens. J Biol Chem 1997;272: 5069–75.
26. Brzozowski AM, Pike ACW, Dauter Z, Hubbard RE, Bonn T, Engström O, et al. Molecular basis of agonism and antagonism in the oestrogen receptor. Nature 1997;389:753–8.
27. Chung JH, Pavlick D, Hartmaier R, Schrock AB, Young L, Forcier B, et al. Hybrid capture-based genomic profiling of circulating tumor DNA from patients with estrogen receptor-positive metastatic breast cancer. Ann Oncol 2017;28:2866–73.
28. Wardell SE, Nelson ER, Chao CA, Mcdonnell DP. Bazedoxifene exhibits antiestrogenic activity in animal models of tamoxifen-resistant breast cancer: implications for treatment of advanced disease. Clin Cancer Res 2013;19: 2420–31.
29. Toy W, Carlson K, Martin T, Razavi P, Berger M, Baselga J, et al. Non-canonical, clinical ESR1 mutations promote resistance to antiestrogen therapies. In: Proceedings of the 2018 San Antonio Breast Cancer Symposium; 2018 Dec 4-8; San Antonio, TX. Philadelphia (PA): AACR; Cancer Res 2019;79(4 Suppl): Abstract nr P5-04-11.
30. Hamilton EP, Wang JS, Pluard TJ, Johnston SRD, Morikawa A, Claire Dees E, et al. Phase I/II trial of H3B-6545, a novel selective estrogen receptor covalent antagonist (SERCA), in estrogen receptor positive (ER+), human epidermal growth factor receptor 2 negative (HER2-) advanced breast cancer. J Clin Oncol 39:15s, 2021 (suppl; abstr 1018).
31. Korpal M, Furman C, Puyang X, Zhang Z, Wu Z, Banka D, et al. Development of H3B-6545, a first-in-class oral selective ER covalent antagonist (SERCA), for the treatment of ERaWT and ERaMUT breast cancer; 2020.
32. Hamilton EP, Wang JS, Pluard T, Johnston SRD, Morikawa A, Dees EC, et al. Phase I/II study of H3B-6545, a novel selective estrogen receptor covalent antagonist (SERCA), in estrogen receptor positive (ER+), human epidermal growth factor receptor-2 negative (HER2-) advanced breast cancer. J Clin Oncol 39:15s, 2021 (suppl; abstr 1018).
33. Eastell R, Hannon RA, Cuzick J, Dowsett M, Clack G, Adams JE. Effect of an aromatase inhibitor on bmd and bone turnover markers: 2-year results of the Anastrozole, Tamoxifen, Alone or in Combination (ATAC) trial (18233230). J Bone Miner Res 2006;21:1215–23.